Engine Compartment UWB Channel Model for Intravehicular Wireless Sensor Networks

Utku Demir, C. Umit Bas, *Member, IEEE*, and Sinem Coleri Ergen, *Member, IEEE*

***Abstract*—Intravehicular wireless sensor network (IVWSN) is a cutting edge research topic that delivers cost reduction, assembly, and maintenance efficiency by removing the wiring harnesses within the vehicle and enables the integration of new sensors into the locations inside a vehicle where cable connection is not possible. Providing energy efficiency through the low-duty-cycle operation and high reliability by exploiting the large bandwidth, ultrawideband (UWB) has been determined to be the most appropriate technology for IVWSNs. We investigate the UWB channel model for IVWSNs within the engine compartment of a vehicle by collecting an extensive amount of data for 19 $\times$ 19 links for different types and conditions of the vehicle. These include a Fiat Linea with engine off, Fiat Linea with engine on, and Peugeot Bipper with engine off. The path-loss exponent is estimated to be around 3.5 without exhibiting much variation when the engine is turned on and for different types of vehicles. The power variation around the expected path loss has lognormal distribution with zero mean and standard deviation in the range of [5.5, 6.3] dB for different types of vehicles with almost no variation when the engine of the same vehicle is turned on. The clustering phenomenon in the power delay profile (PDP) is well represented by a modified Saleh–Valenzuela (SV) model. The interarrival times of the clusters are modeled using a Weibull distribution. The cluster-amplitude and ray-amplitude decay functions are represented with a dual-slope linear model with breakpoint around 26.6 and 5.5 ns, respectively. The parameters of the Weibull distribution and these dual-slope linear models do not vary significantly for different types and conditions of the vehicle. The variations of the observed PDPs around the SV model is well modeled by independent normal random variables with zero mean and with a variance independent of the delay bin, and the type and condition of the vehicle. We propose a simulation model for the UWB channel within the engine compartment based on these findings and validate it by comparing the received energy and root mean square (RMS) delay spread of the generated and observed PDPs.**

***Index Terms*—Channel models, engine compartment, ultrawideband (UWB), vehicle, wireless sensor networks.**

Manuscript received January 21, 2013; revised October 9, 2013; accepted November 22, 2013. Date of publication December 6, 2013; date of current version July 10, 2014. This work was supported by the Marie Curie Reintegration Grant on Intra-Vehicular Wireless Sensor Networks under Grant PIRG06-GA-2009-256441. The review of this paper was coordinated by Prof. C. X. Wang.

U. Demir and S. Coleri Ergen are with the Department of Electrical and Electronics Engineering, Koc University, 34450 Istanbul, Turkey (e-mail: utdemir@ku.edu.tr; sergen@ku.edu.tr).

C. U. Bas was with the Department of Electrical and Electronics Engineering, Koc University, 34450 Istanbul, Turkey. He is now with the Department of Electrical Engineering, University of Southern California, Los Angeles, CA 90089 USA (e-mail: cbas@usc.edu).

Color versions of one or more of the figures in this paper are available online at http://ieeexplore.ieee.org.

Digital Object Identifier 10.1109/TVT.2013.2294357

I. Introduction

THE proliferation of electronic systems within a vehicle, as they are replacing their mechanical or hydraulic counterparts, has led to an increase in the number of sensors monitoring various quantities so as to improve their performance [1]. Since every sensor needs to be wired to an electronic control unit to communicate the sensor information and to the battery of the vehicle to supply power, part cost, maintenance, and assembly problems arise within the vehicle. Removing the wiring not only provides cost reduction but also fuel efficiency due to the decrease in the vehicle weight. Moreover, such wireless technology allows the integration of new sensors into vehicle locations where cable connection is not possible [2]. The first adoption of wireless sensor networks within the vehicle is expected to be through these new sensor technologies and noncritical vehicle applications either requiring a lot of wiring, such as park sensors, or not operating efficiently due to wiring, such as steering-wheel angle sensors. Once the performance and reliability of these applications are proven by extensive tests on the road, the wiring can be removed for more critical applications such as an antilock braking system [3].

Among alternative communication technologies such as radio-frequency identification (RFID) [4], narrow band [5], [6], and spread spectrum [7], [8], UWB has been demonstrated to satisfy the high reliability constraints of IVWSN applications by exploiting the large bandwidth and their energy efficiency constraints through the low-duty-cycle operation. UWB is defined as transmission with bandwidth more than $<$ 500 MHz and 20% of the center frequency. This huge bandwidth enables UWB transmission to be resistant against multipath fading and signal power attenuation, providing robust communication at low transmission power and a high communication rate.

To design a well-functioning UWB system, an appropriate channel model should be extracted. The vast literature on UWB channel models developed for indoor [9]–[13], outdoor [14]–[17], around the human body [18], [19] or industrial environments [20] cannot be applied for IVWSNs since the vehicle is very different from these environments containing a large number of metal reflectors at a short distance and with a lot of vibrations resulting in a dense multipath. The UWB channel models developed for different parts of the vehicle, including engine compartment [21], [22], beneath the chassis [21], [22], passenger compartment [23]–[26], and trunk [27], on the other hand, are extracted based on the measurements in a limited number of locations, i.e., 24 locations at maximum, without building a detailed simulation model and testing the robustness of the model under different scenarios such as different types

and conditions of vehicles. Only recently has such a detailed model been proposed and tested beneath the chassis of the vehicle [28], [29].

The goal of this paper is to propose a robust UWB channel model within the engine compartment of the vehicle by collecting data at 19 × 19 locations for two types of vehicles under different scenarios. The engine compartment channel measurement campaigns in [21] and [22] are performed at only 5 and 9 locations, respectively, decreasing the reliability of the measurement results. Moreover, they do not propose a simulation model for the UWB engine compartment channel but only derive a subset of the required channel model parameters. The original contributions of this paper are as follows.

- We derive the distributions, parameters, and dependence relations related to the UWB engine-compartment channel model, including the path loss and power variation around the expected path loss; the distribution of the cluster interarrival times and the dependence of the cluster amplitude and cluster decay rate on the cluster arrival times in the Saleh–Valenzuela (SV) model; and the probabilistic distribution of the variation of the observed PDPs around the SV model. This is the first work to provide a complete analysis of the distributions, parameters, and dependence relations related to the UWB engine-compartment channel model.
- We generate the simulation model for the UWB channel within the engine compartment and validate the model by comparing the received energy and RMS delay spread obtained from the simulation and experimental data. This is the first simulation model generated for the UWB engine-compartment channel.
- We analyze the validity of the simulation model and the sensitivity of the model parameters for different vehicle types and conditions. This is the first work to analyze the validity of the engine channel model across a wide range of scenarios.

The remainder of this paper is organized as follows. Section II provides the experimental setup. Section III presents the path loss and power variation around the expected path loss for different vehicle types and conditions. In Section IV, the probabilistic distribution of the SV parameters, including interarrival times, cluster amplitudes, and ray decay rates for different vehicle types and conditions, are derived. Section V presents the statistics of the difference between the observed PDPs and the SV model for different vehicle types and conditions. The simulation model for the UWB channel within the engine compartment and the validation of the model are given in Section VI. The main results are summarized in Section VII.

II. Experimental Setup

The channel measurement data are collected by using an Agilent 8719ES vector network analyzer (VNA) covering the frequency range of [3.1, 10.6] GHz using 1601 points. The UWB antennas used in the experiments are omnidirectional and directed toward the bottom of the vehicle. The antennas are connected to the VNA via low-loss coaxial cables. The VNA is calibrated for each frequency band to eliminate the effect of

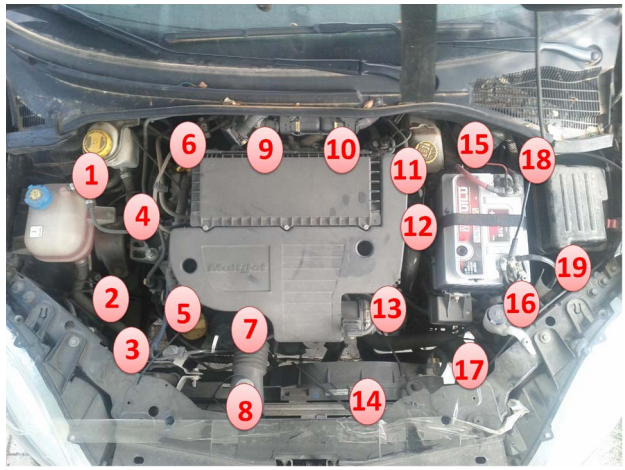

Fig. 1. Sensor locations within the engine of Fiat Linea.

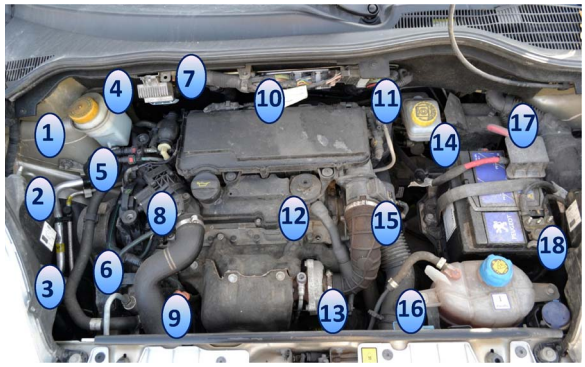

Fig. 2. Sensor locations within the engine of Peugeot Bipper.

signal distortions by the cables. The coaxial cable may influence the parameters of the UWB antennas due to their small size. However, we observed that the measurements of the VNA remain stable upon the movement of the cables, demonstrating that they do not radiate enough energy to alter our results. The return loss at the antennas has been measured to be negligible across the band of interest.

We performed our channel measurement in a Fiat Linea and a Peugeot Bipper between every pair of the sensor locations shown in Figs. 1 and 2, respectively, for two scenarios where the engine is off and where the engine is on. The sensor locations are chosen to cover the whole area within the engine compartment.

VNA provides the complex transfer function $H(f)$. We process this transfer function to obtain a reliable PDP in Matlab as follows.

- $H(f)$ is passed through the Hamming window to decrease the sidelobes and then the Inverse Fourier Transform (IFFT) to generate the impulse response $h(t)$ at the output. The PDP is then computed as $|h(t)|^2$ normalized with respect to the reference PDP measured between a transmitter–receiver pair at the reference distance.
- The PDP is shifted by the corresponding propagation delay to the left to guarantee that the first bin is aligned with the first multipath component.

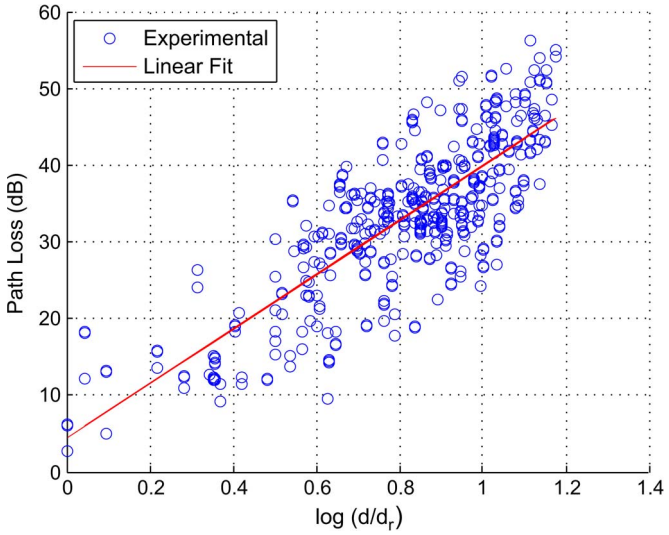

Fig. 3. Dependence of the path loss on the distance within the engine compartment of Fiat Linea when the engine is off.

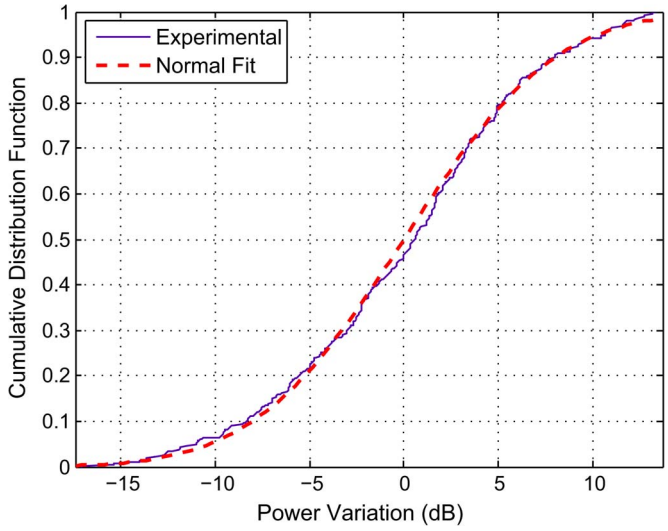

Fig. 4. CDF of the power variation.

- The delay axis of the PDP is quantized into bins. The received power is integrated within each bin. The bin width is chosen to contain five samples to make a good compromise between high delay resolution and noise reduction.

The goal of this paper is to derive and validate the simulation model for the resulting PDP.

III. Path Loss and Power Variation

The path loss between a transmitter–receiver pair originates from both the free-space attenuation and the level of absorption, reflection, diffraction, and refraction in the engine compartment. The path-loss model is given as

$$\mathrm{PL}_{[\mathrm{dB}]}(d) = \mathrm{PL}_{[\mathrm{dB}]}(d_r) + 10n\log_{10}\left(\frac{d}{d_r}\right) + N \qquad (1)$$

where $\mathrm{PL}_{[\mathrm{dB}]}(d)$ and $\mathrm{PL}_{[\mathrm{dB}]}(d_r)$ are the path loss at distance d and at reference distance $d_r = 7$ cm in decibels, respectively; n is the path-loss exponent; and N is a zero-mean normal random variable with standard deviation σ_N [30].

Fig. 3 shows the path loss as a function of the distance along with the best linear fit obeying (1) for the engine compartment of Fiat Linea when the engine is off. The path-loss exponent n is found to be 3.5.

Fig. 4 shows the cumulative distribution function (cdf) of the experimental power variation in decibels along with the least squares fit of the cdf of the normal random variable for the engine compartment of Fiat Linea when the engine is off. The power variation is calculated by finding the difference between the measured path-loss values and the best linear fit in Fig. 3, which is represented by N in (1). We observe that the frequently used normal random variable is an appropriate model for the engine compartment with standard deviation $\sigma_N = 6.3$ dB.

Table I shows the parameters of the path loss and power variation for three scenarios: "Linea off" represents Fiat Linea with engine off, "Linea on" corresponds to Fiat Linea with engine on, "Bipper off" is for Peugeot Bipper with engine off.

TABLE I
Parameters of the Path Loss and Power Variation. The Unit of $\mathrm{PL}_{[\mathrm{dB}]}(d_r)$ and σ_N are in Decibels

Scenario	n	$PL_{[\mathrm{dB}]}(d_r)$	σ_N
Linea off	3.5369	4.436	6.25
Linea on	3.5594	4.194	6.24
Bipper off$_1$	2.8090	10.63	5.31
Bipper off$_2$	3.563	4.436	5.58

Subscript 1 corresponds to the case where the values of n, $\mathrm{PL}_{[\mathrm{dB}]}(d_r)$, and σ_N are obtained by the curve fitting of the measured data to (1) in a minimum mean square error sense, whereas subscript 2 corresponds to the case where the same $\mathrm{PL}_{[\mathrm{dB}]}(d_r)$ value as that of the "Linea off" is used and where n and σ_N values are obtained by the curve fitting of the measured data to (1) in a minimum mean square error sense. The reason for using the latter estimation method is the expectation that the path loss at the reference distance would not be so different for different engines. As also observed in Fig. 5, this method does not increase the standard deviation σ_N significantly and allows us to obtain a more generic path-loss model with similar estimated n, $\mathrm{PL}_{[\mathrm{dB}]}(d_r)$, and σ_N values for different types of vehicles. We can therefore conclude that turning the engine on and the type of the vehicle do not affect the path-loss parameters significantly.

In [22], Niu *et al.* stated that the estimated path-loss parameters are $n = 1.51$, $\mathrm{PL}_{[\mathrm{dB}]}(d_r) = 6.32$ dB, and $\sigma_N = 3$ dB based on the data collected from nine measurement pairs in the engine compartment of the GM Escalade, but the corresponding values change to $n = 4.73$, $\mathrm{PL}_{[\mathrm{dB}]}(d_r) = 35.15$ dB, and $\sigma_N = 1.06$ dB if the measurement from two positions are excluded, which decreases the reliability of the estimated values. Our estimated values are robust to the exclusion of a few measurement points due to the collection of a large amount of data within the engine.

IV. Impulse Response Analysis

The PDP in the engine compartment consists of many clusters, as shown in Fig. 6. The PDP in this figure belongs to

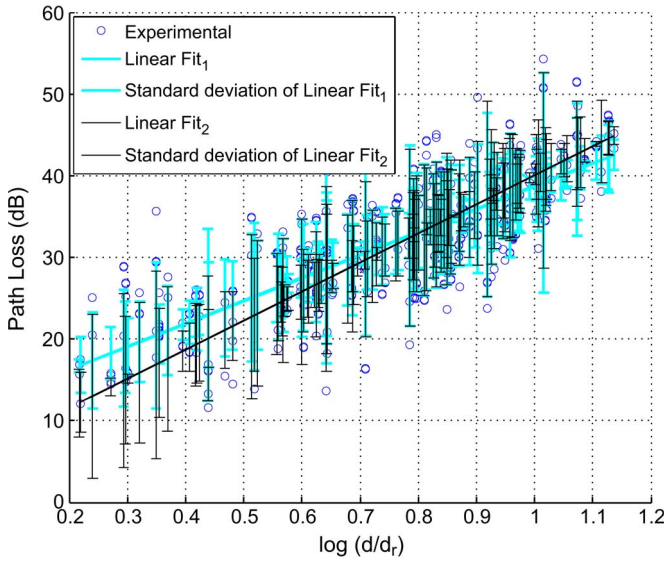

Fig. 5. Dependence of the path loss on the distance within the engine compartment of Peugeot Bipper when the engine is off.

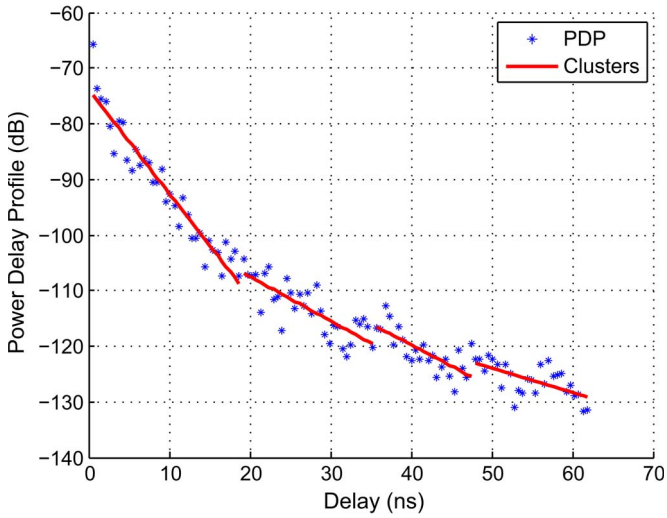

Fig. 6. Typical PDP in the engine compartment [receiver 1 and transmitter 4 in the engine compartment of Fiat Linea shown in (Fig. 1)].

the receiver at location 1 and transmitter at location 4 in the engine compartment of the Fiat Linea shown in Fig. 1. We determined the arrival time of each cluster by using the automatic clustering algorithm presented in [31] and then validated the accuracy of the algorithm by visual inspection. Assuming that the slope changes at the beginning of each cluster, the automatic clustering algorithm identifies the change points of the partial slopes of the impulse response.

The arrival time and amplitude of the clusters in the PDP is modeled by using a modified SV model [9], which is frequently used to represent the behavior of the random clusters in UWB channels. The SV model defines the impulse response of a system as

$$y(t) = \sum_{b=0}^{B} \sum_{a=0}^{A} \alpha_{b,a} e^{j\phi_{b,a}} \sigma(t - T_b - \tau_{b,a}) \qquad (2)$$

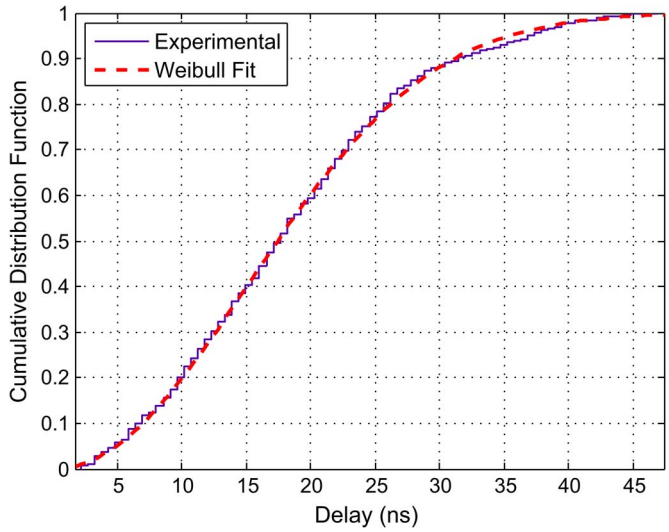

Fig. 7. CDF of the interarrival times of the clusters.

where $\alpha_{b,a}$ is the gain and $\phi_{b,a}$ is the phase of the ath component in the bth cluster, T_b is the delay of the bth cluster, $\tau_{b,a}$ is the delay of the ath multipath component in the bth cluster relative to the bth cluster arrival time T_b, B is the number of clusters, and A is the number of the multipath components within a cluster. The phases $\phi_{b,a}$ are uniformly distributed in the range of $[0, 2\pi]$.

In the classical SV model, the distributions of the cluster arrival times are given by a Poisson process so that the intercluster arrival times are exponentially distributed. This model also uses a Poisson process for the ray arrival times within each cluster. Moreover, both the amplitude of the clusters and the amplitude of the rays within each cluster are decreasing exponentially with the arrival time. The decay rate of the clusters and rays are different but are fixed and independent of their arrival time. We will now analyze the distribution of the intercluster arrival times, the dependence of the amplitude of the clusters, and the decay rate of the rays within each cluster on the arrival times of the clusters for the UWB channel within the engine compartment of the vehicle. Since each delay bin contains a significant amount of energy due to the dense arrival of the multipath components in the engine compartment, we do not analyze the distributions of the ray arrivals within each cluster but assume a realization of the impulse response based on a tapped delay line model with regular tap spacing.

A. *Interarrival Times of Clusters*

Fig. 7 shows the cdf of the interarrival times of the clusters for the engine compartment of Fiat Linea when the engine is off. We observed that the Weibull distribution matches better with the experimental cdf than the exponential distribution used in the classical SV model because of the nonrandom local configuration of the engine compartment [19]. Kolmogorov–Smirnov (KS) test results with a 95% confidence interval for Weibull and exponential distributions are 0.0238 and 0.2338, respectively, justifying this observation. (The KS test is a nonparametric test determining the goodness of a reference

TABLE II
SHAPE AND SCALE PARAMETERS OF THE WEIBULL FIT FOR THE INTERARRIVAL TIMES OF THE CLUSTERS, AND THE KS TEST RESULT WITH A 95% CONFIDENCE INTERVAL FOR THE WEIBULL AND EXPONENTIAL DISTRIBUTIONS WITH THE EXPERIMENTAL INTERARRIVAL TIMES OF THE CLUSTERS DENOTED BY KS_W AND KS_E, RESPECTIVELY. THE UNIT OF λ IS IN NANOSECONDS

Scenario	k	λ	KS_W	KS_E
Linea off	2.06	20.7879	0.0238	0.2338
Linea on	2.622	24.4654	0.0484	0.294
Bipper off	2.292	21.3313	0.0541	0.2687

distribution for the experimental data.) The Weibull distribution is given as

$$f(x) = \begin{cases} \frac{k}{\lambda}\left(\frac{x}{\lambda}\right)^{k-1} e^{-(x/\lambda)^k}, & x \geq 0 \\ 0, & x < 0 \end{cases} \tag{3}$$

where $k > 0$ is the shape parameter, and $\lambda > 0$ is the scale parameter of the distribution. The shape and scale parameters of the Weibull distribution are found to be $k = 2.06$ and $\lambda = 20.79$ ns, respectively.

Table II shows the shape and scale parameters of the Weibull fit for the interarrival times of the clusters and the KS test result with a 95% confidence interval for Weibull and exponential distributions with the experimental interarrival times of the clusters for three scenarios, as described in detail for Table I. The KS test results justify that the Weibull distribution is a better fit than the exponential distribution for different types and conditions of the vehicle. Moreover, the shape and scale parameters of the Weibull fit for the interarrival times of the clusters do not vary significantly when the engine of the vehicle is turned on or the vehicle type is different: The KS statistic for the Weibull fit of "Linea off" and "Linea on" cases is 0.1957, whereas that for the Weibull fit of "Linea off" and "Bipper off" cases is 0.063. (The KS statistic for two empirical distribution functions F_1 and F_2 is defined as $\sup_x |F_1(x) - F_2(x)|$).

The previous work on the engine-compartment UWB channel model does not analyze the suitability of alternative distributions for the interarrival times of the clusters, but it is clear that exponential distribution does not fit well their experimental data either [21], [22]. On the other hand, in [28] and [29], we similarly observe that the Weibull fit is a better fit for the interarrival times of the clusters beneath the chassis. Scale parameter λ beneath the chassis is less than that of the engine compartment, which is less than 15 ns for the same scenarios, and the shape parameter k beneath the chassis is similar to that of the engine compartment but with much larger variation from 1.9 to 2.8 for the same scenarios.

B. Cluster-Amplitude Decay Function

Fig. 8 shows the dependence of the cluster amplitude on the cluster arrival time for the engine compartment of Fiat Linea when the engine is off. The cluster amplitude denotes the power of the first bin of the cluster relative to the total energy. The reason for normalizing the cluster amplitudes by the total energy is to eliminate the dependence on the distance.

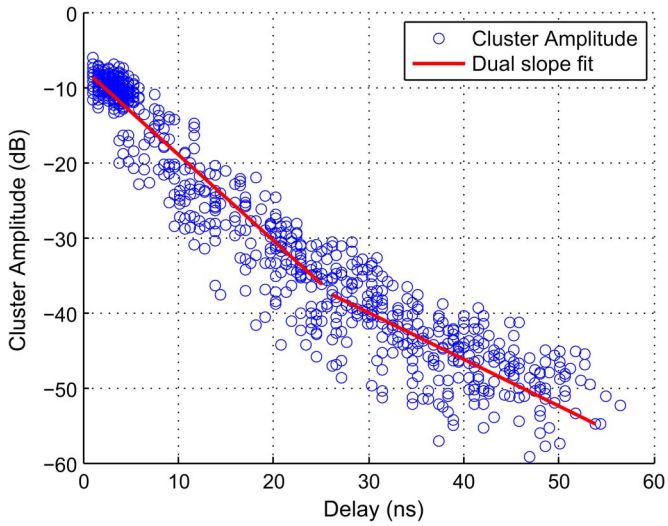

Fig. 8. Dependence of the cluster amplitude on the cluster arrival time.

TABLE III
PARAMETERS OF THE CLUSTER-AMPLITUDE DECAY FUNCTION. THE UNIT OF c_{11} AND c_{21} IS IN DECIBELS PER NANOSECONDS. THE UNIT OF c_{10} AND c_{20} IS IN DECIBELS. THE UNIT OF τ_{bc} IS IN NANOSECONDS

Scenario	c_{11}	c_{10}	c_{21}	c_{20}	τ_{bc}
Linea off	-1.143	-7.5	-0.619	-21.45	26.6
Linea on	-1.256	-7.38	-0.645	-20.15	25
Bipper off	-1.223	-6.728	-0.633	-18.67	28

The cluster-amplitude decay function is modeled by using the dual-slope linear model as

$$f(T_b) = \begin{cases} c_{11} \cdot T_b + c_{10}, & T_b \leq \tau_{bc} \\ c_{21} \cdot T_b + c_{20}, & T_b > \tau_{bc} \end{cases} \tag{4}$$

where $f(T_b)$ represents the power of the first bin of the cluster arriving at delay T_b relative to the total energy in decibels; τ_{bc} is the breakpoint between the two lines; c_{11} and c_{21} are the slopes of the least squares fit line before and after the breakpoint, respectively; and c_{10} and c_{20} are the cluster-amplitude axis intercept point of the least squares fit line before and after the breakpoint, respectively. The parameters of the model are estimated as follows: $c_{11} = -1.143$ dB/ns, $c_{10} = -7.5$ dB, $c_{21} = -0.619$ dB/ns, $c_{20} = -21.45$ dB, and $\tau_{bc} = 26.6$ ns.

Table III shows the parameters of the cluster-amplitude decay function for three scenarios, as described in detail for Table I. We observe that these parameters do not change significantly for different types and conditions of the vehicle. The previous work on the engine-compartment UWB channel model provide a linear fit for the cluster-amplitude decay function with much slower decay, a slope of -0.323 dB/ns, which is based on the data collected from at most nine measurement points [21], [22]. On the other hand, [28] and [29] similarly observe a dual-slope linear model for the cluster-amplitude decay function beneath the chassis. Although the slope of the first line is comparable for both the engine compartment and beneath the chassis, the slope of the second line is slightly higher for the engine than beneath the chassis due to the large number of obstructing elements densely deployed within the engine compartment at short distance.

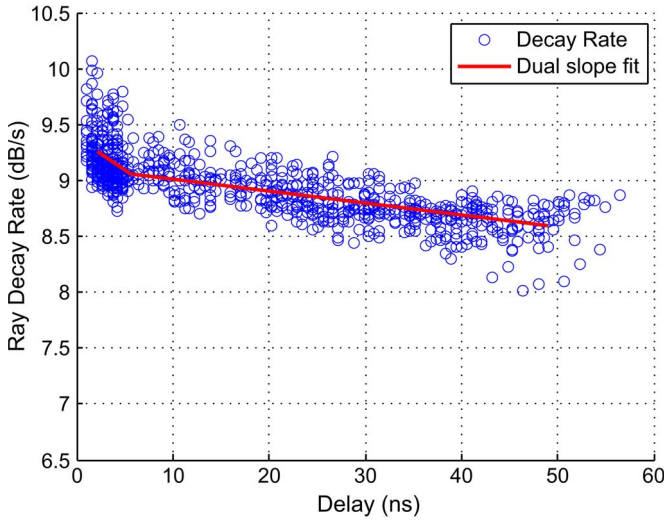

Fig. 9. Dependence of the ray decay rate on the cluster arrival time.

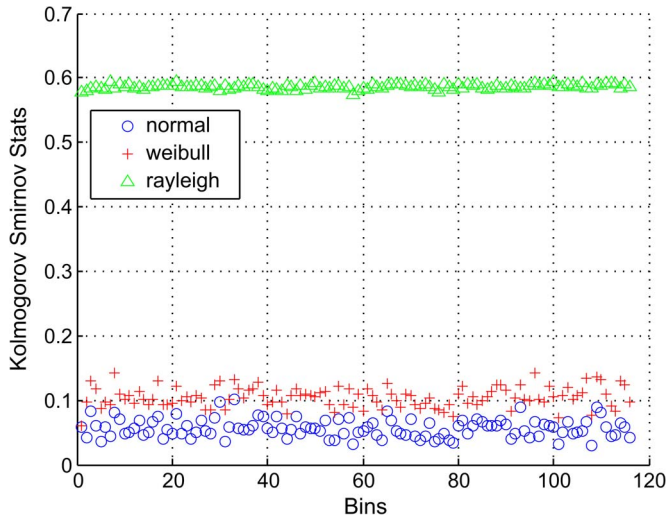

Fig. 10. Results of the KS test with a 95% confidence interval for the difference between the observed PDPs and the SV model in each delay bin.

TABLE IV
PARAMETERS OF THE RAY-AMPLITUDE DECAY FUNCTION. THE UNIT OF d_{11} AND d_{21} IS dB/ns^2. THE UNIT OF d_{10} AND d_{20} IS IN DECIBELS PER NANOSECONDS. THE UNIT OF τ_{br} IS IN NANOSECONDS

Scenario	d_{11}	d_{10}	d_{21}	d_{20}	τ_{br}
Linea off	-0.057	9.381	-0.01	9.121	5.56
Linea on	-0.05	9.323	-0.013	9.108	5.86
Bipper off	-0.054	9.306	-0.008	8.98	5.33

C. Ray-Amplitude Decay Function

Once the power of the first bin of all the clusters is determined by calculating the cluster amplitude given in (4), the ray decay rate of these clusters need to be specified so that we can calculate the power of all the bins within these clusters. Assuming that the decay in each cluster is linear, as shown in Fig. 6, the power of the ath bin of the bth cluster is formulated as

$$g(T_b + \tau_{b,a}) = f(T_b) - \xi(T_b)\tau_{b,a} \tag{5}$$

where $g(T_b + \tau_{b,a})$ is the power of the ath bin of the bth cluster arriving at delay T_b relative to the total energy in decibels, and $\xi(T_b)$ is the decay rate of the cluster arriving at delay T_b in decibels.

Fig. 9 shows the dependence of the ray-amplitude decay function ξ on the cluster arrival time T_b for the engine compartment of Fiat Linea when the engine is off. The ray-amplitude decay function is modeled by using the dual-slope linear model as

$$\xi(T_b) = \begin{cases} d_{11} \cdot T_b + d_{10}, & T_b \leq \tau_{br} \\ d_{21} \cdot T_b + d_{20}, & T_b > \tau_{br} \end{cases} \tag{6}$$

where τ_{br} is the breakpoint between the two lines; d_{11} and d_{21} are the slopes of the least squares fit line before and after the breakpoint respectively; and d_{10} and d_{20} are the ray decay rate axis intercept point of the least squares fit line before and after the breakpoint, respectively. The parameters of the model are estimated as follows: $d_{11} = -0.057$ dB/ns^2, $d_{10} = 9.381$ dB/ns, $d_{21} = -0.01$ dB/ns^2, $d_{20} = 9.121$ dB/ns, and $\tau_{br} = 5.56$ ns.

Table IV shows the parameters of the ray-amplitude decay function for three scenarios, as described in detail for Table I. Similar to the cluster-amplitude decay function, we observe that the parameters of the ray-amplitude decay function do not vary significantly for different vehicle types and conditions. The previous work on the engine-compartment UWB channel model does not provide the dependence of the ray-amplitude decay on the cluster arrival times [21], [22]. On the other hand, the works in [28] and [29] similarly observe a dual-slope linear model for the ray-amplitude decay function beneath the chassis. However, the breakpoint of the dual-slope linear model beneath the chassis is around 27 ns, which is much larger than that of the engine compartment.

We have also investigated whether the power-law fit provides better results than the exponential fit given in (6). Although some of the studies on the UWB channel model for the environments containing a large number of metallic reflectors [14], [20] report that the ray decay follows a power-law fit rather than an exponential fit, the MSE of the power law fit is either greater or very close to that of the exponential fit in the engine compartment, i.e., the MSEs of the exponential fit are 0.0334, 0.0296, and 0.0328, whereas the MSEs of the power-law fit are 0.0326, 0.0300, and 0.0319 in unit of $(\text{dB/ns})^2$ for "Linea off," "Linea on," and "Bipper off" cases, respectively. This validates the exponential fit dual-slope linear model given in (6).

V. VARIATION OF POWER DELAY PROFILE AROUND THE SALEH–VALENZUELA MODEL

The SV model is used to build the clustered impulse response, as shown with the use of lines in Fig. 6. However, the actual impulse response varies around this SV model. To understand the distribution of these variations, we analyzed the best fit for these variations in each delay bin.

Fig. 10 shows the results of the KS test with a 95% confidence interval for normal, Weibull, and Rayleigh distributions for the engine compartment of Fiat Linea when the engine is off. We observe that normal distribution is the best distribution in almost all the delay bins. Fig. 11 shows the mean and standard deviation of the best-fit normal distribution in all the delay bins.

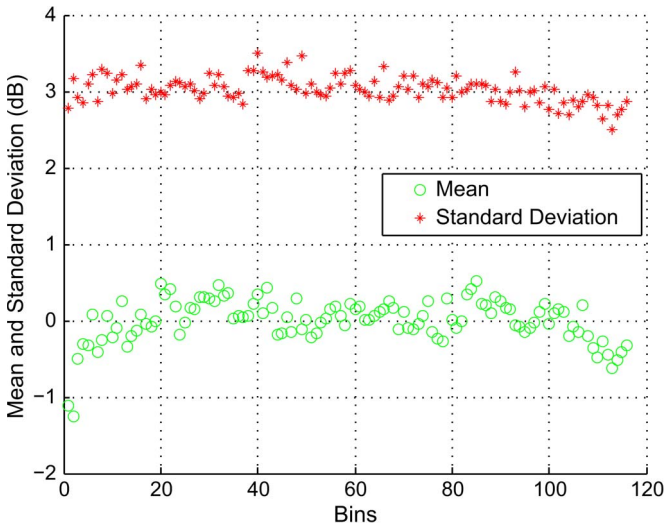

Fig. 11. Mean and standard deviation of the difference between the observed PDPs and the SV model in each delay bin.

TABLE V
AVERAGE STANDARD DEVIATION OF THE VARIATION OF THE PDP AROUND THE SV MODEL. THE UNIT OF σ_z IS IN DECIBELS

Scenario	σ_z
Linea off	3.03
Linea on	3.02
Bipper off	3.13

We observe that the mean and standard deviation is independent of the delay with average values $\mu_z = 0$ dB and $\sigma_z = 3.03$ dB, respectively. The average of the mean value 0 demonstrates that the SV model correctly represents the measured PDPs.

We observed similar behavior in the variation of the PDPs around the SV model when the engine of Fiat Linea is turned on and for Peugeot Bipper. Table V shows the average standard deviation of the variation of the PDP around SV model for three scenarios, as described in detail for Table I. We observe that the average standard deviation of the variation of the PDP around the SV model is independent of not only the delay bin but also the type and condition of the vehicle.

VI. SIMULATION MODEL

A. Generation of Simulation Model

We now describe the algorithm for generating the simulation model for the engine-compartment UWB channel based on our findings in Sections III–V. The algorithm is given in Fig. 12 with the details explained in the following.

- The cluster arrival times are calculated first based on our findings in Section IV-A. The arrival time of the first cluster is at the propagation delay $T_0 = \mathrm{d/c}$, where d is the distance between the transmitter and receiver, and c is the speed of light. The arrival time of the following clusters are calculated by computing the random value from the Weibull distribution with the parameters provided in Table II and by adding to the previous arrival time. This continues as long as the computed arrival times are less than the maximum delay spread.

Input: Distance between transmitter and receiver
Output: Power delay profile between transmitter and receiver

1: begin
2: $T_0 = d/c, B = 0$;
3: while $T_B \leq$ Delay spread
4: $T_{B+1} = T_B + weibull(\lambda, k)$;
5: $B = B + 1$;
6: end
7: Calculate the cluster amplitudes by using dual slope linear model $f(T_b - T_0)$ for $b = 0 : (B-1)$
8: Calculate the ray amplitudes within the clusters by using the function $g(T_b - T_0 + \tau_{b,a}) = f(T_b - T_0) - \xi(T_b - T_0)\tau_{b,a}$ for $b = 0 : (B-1)$ and $\tau_{b,a} \in [0, T_{b+1} - T_b]$
9: Scale the PDP according to the path loss function
10: Add Gaussian random variable $N(0, \sigma_z^2)$ to each delay bin of PDP
11: end

Fig. 12. Algorithm for generating the simulation model for the engine-compartment UWB channel.

- The power of the first bin of the cluster relative to the total energy, i.e., cluster amplitude, corresponding to the arrival time of each cluster is then computed based on our findings in Section IV-B. Since the derivation of the cluster-amplitude decay function assumes that the PDP is shifted to the left by the propagation delay, the cluster amplitude is calculated by using the dual-slope linear model given in (4) evaluated at $T_b - T_0$ for $b = 0 : (B-1)$ with the parameters provided in Table III.
- The power of the following bins of the cluster are computed based on our findings in Section IV-C. The power of the ath bin of the bth cluster is calculated by using $g(T_b - T_0 + \tau_{b,a}) = f(T_b - T_0) - \xi(T_b - T_0)\tau_{b,a}$, where $\xi(T_b - T_0)$ is the ray-amplitude decay function modeled by using the dual-slope linear model formulated in (6) with the parameters given in Table IV.
- Since up to now, the goal was to identify the general shape of the impulse response; the power of all the bins are derived based on the normalized PDPs. The next step in generating the simulation model is to scale the PDP by using the path-loss model provided in (1) with the parameters summarized in Table I, as derived in Section III.
- The random variations of the observed PDP around the SV model are added to each delay bin based on our findings in Section V. The final PDP is calculated by adding independent normal random variables with the parameters summarized in Table V to each delay bin of the PDP.

B. Validation of Simulation Model

We implemented the simulation model described in Section VI-A in Matlab for all three scenarios including Fiat Linea with engine off, Fiat Linea with engine on, and Peugeot Bipper with engine off, and validated the model by comparing the resulting cdf of the receive energy and RMS delay spread of the simulated and experimental PDPs.

Fig. 13 shows the cdf of the received energy of the experimental and simulated PDPs for the engine compartment of Fiat Linea when the engine is off. We observe that the experimental and simulated PDPs are in good agreement in terms of received energy with KS statistic equal to 0.0877. We observe similar

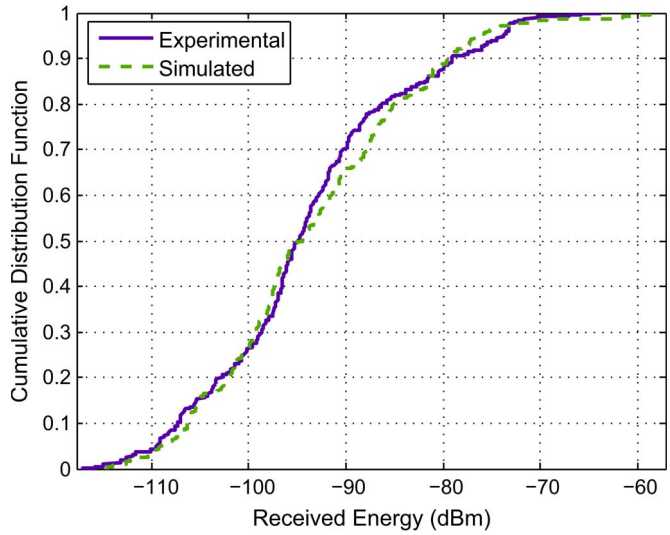

Fig. 13. CDF of the received energy of the experimental and simulated PDPs.

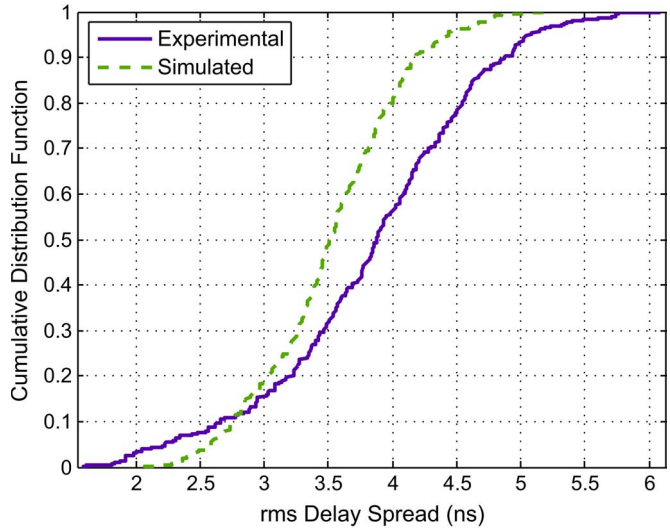

Fig. 14. CDF of the RMS delay spread of the experimental and simulated PDPs.

agreement for Fiat Linea with engine on and Peugeot Bipper with engine off scenarios with KS statistics equal to 0.0936 and 0.0523, respectively.

Fig. 14 shows the cdf of the RMS delay spread of the experimental and simulated PDPs for the engine compartment of Fiat Linea when the engine is off. The RMS delay spread of the simulated PDPs is a little narrower than that of the experimental PDPs with KS statistic equal to 0.2661. This is probably because of the approximation of the cluster-amplitude and ray-amplitude decay functions by dual-slope linear models, despite the large variations around this model. We observe similar behavior for the Fiat Linea with engine on and Peugeot Bipper with engine off scenarios with KS statistics equal to 0.2398 and 0.0817, respectively.

VII. Conclusion

We investigated the UWB channel model for IVWSNs within the engine compartment of the vehicle by collecting an extensive amount of data for 19×19 links for different types and conditions of the vehicle. These include a Fiat Linea with engine off, Fiat Linea with engine on, and Peugeot Bipper with engine off. We derived the distributions, parameters, and dependence relations related to the UWB engine-compartment channel model, including the path loss and power variation around the expected path loss; the distribution of the cluster interarrival times and the dependence of the cluster amplitude and cluster decay rate on the cluster arrival times in the SV model; and the probabilistic distribution of the variation of the observed PDPs around the SV model. We generated the simulation model for the UWB channel within the engine compartment and validated the model by comparing the received energy and RMS delay spread obtained from the simulation and experimental data. The main findings of this paper are as follows.

- The path-loss exponent is estimated to be around 3.5 without exhibiting much variation when the engine is turned on and for different types of vehicles.
- The power variation around the expected path loss has lognormal distribution with mean 0 and standard deviation in the range of [5.5, 6.3] dB for different types of vehicles with almost no variation when the engine of the same vehicle is turned on.
- The clustering phenomenon in the PDP is well represented by a modified SV model. The interarrival times of the clusters are modeled using the Weibull distribution. The cluster-amplitude and ray-amplitude decay functions are represented with a dual-slope linear model with breakpoint around 26.6 and 5.5 ns, respectively. The parameters of the Weibull distribution and these dual-slope linear models do not vary significantly for different types and conditions of the vehicle.
- The variations of the observed PDPs around the SV model are well represented by independent normal random variables with zero mean and variance that is independent of the delay bin, and the type and condition of the vehicle.

The small variations of the model parameters for different types and conditions of the vehicle demonstrate the reliability of the proposed simulation model built based on an extensive set of measurements.

In the future, we plan to investigate the UWB channel model for different parts of the vehicle including the passenger compartment and side of the vehicle, and the time variations of the UWB channel within the vehicle.

References

[1] N. Navet, Y. Song, F. Simonot-Lion, and C. Wilwert, "Trends in automotive communication systems," *Proc. IEEE*, vol. 93, no. 6, pp. 1204–1223, Jun. 2005.

[2] S. C. Ergen, A. Sangiovanni-Vincentelli, X. Sun, R. Tebano, S. Alalusi, G. Audisio, and M. Sabatini, "The tire as an intelligent sensor," *IEEE Trans. Comput.-Aided Design Integr. Circuits Syst.*, vol. 28, no. 7, pp. 941–955, Jul. 2009.

[3] W. Niu, J. Li, S. Liu, and T. Talty, "Intra-vehicle ultra-wideband communication testbed," in *Proc. IEEE MILCOM*, Oct. 2007, pp. 1–6.

[4] O. Tonguz, H. Tsai, C. Saraydar, T. Talty, and A. Macdonald, "Intra-car wireless sensor networks using rfid: Opportunities and challenges," in *Proc. IEEE Mobile Netw. Veh. Environ.*, May 2007, pp. 43–48.

[5] H. Tsai, W. Viriyasitavat, O. Tonguz, C. Saraydar, T. Talty, and A. Macdonald, "Feasibility of in-car wireless sensor networks: A statistical evaluation," in *Proc. IEEE SECON*, Jun. 2007, pp. 101–111.
[6] A. Moghimi, H. Tsai, C. Saraydar, and O. Tonguz, "Characterizing intra-car wireless channels," *IEEE Trans. Veh. Technol.*, vol. 58, no. 9, pp. 5299–5305, Nov. 2009.
[7] M. Ahmed, C. U. Saraydar, T. Elbatt, J. Yin, T. Talty, and M. Ames, "Intra-vehicular wireless networks," in *Proc. IEEE GLOBECOM*, Nov. 2007, pp. 1–9.
[8] H. Tsai, O. Tonguz, C. Saraydar, T. Talty, M. Ames, and A. Macdonald, "Zigbee-based intra-car wireless sensor networks: A case study," *IEEE Wireless Commun.*, vol. 14, no. 6, pp. 67–77, Dec. 2007.
[9] A. Saleh and R. A. Valenzuela, "A statistical model for indoor multipath propagation," *IEEE J. Sel. Areas Commun.*, vol. 5, no. 2, pp. 128–137, Feb. 1987.
[10] D. Cassioli, M. Z. Win, and A. F. Molisch, "The ultra-wide bandwidth indoor channel: From statistical model to simulations," *IEEE J. Sel. Areas Commun.*, vol. 20, no. 6, pp. 1247–1257, Aug. 2002.
[11] B. M. Donlan, D. R. McKinstry, and R. M. Buehrer, "The uwb indoor channel: Large and small scale modeling," *IEEE Trans. Wireless Commun.*, vol. 5, no. 10, pp. 2863–2873, Oct. 2006.
[12] S. S. Ghassemzadeh, R. Jana, C. W. Rice, W. Turin, and V. Tarokh, "Measurement and modeling of an ultra-wide bandwidth indoor channel," *IEEE Trans. Commun.*, vol. 52, no. 10, pp. 1786–1796, Oct. 2004.
[13] S. S. Ghassemzadeh, L. J. Greenstein, T. Sveinsson, A. Kavcic, and V. Tarokh, "Uwb delay profile models for residential and commercial indoor environments," *IEEE Trans. Veh. Technol.*, vol. 54, no. 4, pp. 1235–1244, Jul. 2005.
[14] J. Lee, "Uwb channel modeling in roadway and indoor parking environments," *IEEE Trans. Veh. Technol.*, vol. 59, no. 7, pp. 3171–3180, Sep. 2010.
[15] A. F. Molisch, D. Cassioli, C.-C. Chong, S. Emami, A. Fort, B. Kannan, J. Karedal, J. Kunisch, K. Siwiak, and M. Z. Win, "A comprehensive standardized model for ultrawideband propagation channels," *IEEE Trans. Antennas Propag.*, vol. 54, no. 11, pp. 3151–3166, Nov. 2006.
[16] C. W. Kim, X. Sun, L. C. Chiam, B. Kannan, F. P. S. Chin, and H. K. Garg, "Characterization of ultra-wideband channels for outdoor office environment," in *Proc. IEEE WCNC*, Mar. 2005, pp. 950–955.
[17] C. F. Souza and J. C. R. D. Bello, "Uwb signals transmission in outdoor environments for emergency communications," in *Proc. IEEE Comput. Sci. Eng. Workshop*, Jul. 2008, pp. 343–348.
[18] Y. Chen, J. Teo, J. Y. Lai, E. Gunawan, K. S. Low, C. B. Soh, and P. B. Rapajic, "Cooperative communications in ultra-wideband wireless body area networks: Channel modeling and system diversity analysis," *IEEE J. Sel. Areas Commun.*, vol. 27, no. 1, pp. 5–16, Jan. 2009.
[19] A. Fort, J. Ryckaert, C. Desset, P. Doncker, P. Wambacq, and L. Biesen, "Ultra-wideband channel model for communication around the human body," *IEEE J. Sel. Areas Commun.*, vol. 24, no. 4, pp. 927–933, Apr. 2006.
[20] J. Karedal, S. Wyne, P. Almers, F. Tufvesson, and A. F. Molisch, "A measurement-based statistical model for industrial ultra-wideband channels," *IEEE Trans. Wireless Commun.*, vol. 6, no. 8, pp. 3028–3037, Aug. 2007.
[21] W. Niu, J. Li, and T. Talty, "Intra-vehicle uwb channel measurements and statistical analysis," in *Proc. IEEE GLOBECOM*, Dec. 2008, pp. 1–5.
[22] W. Niu, J. Li, and T. Talty, "Ultra-wideband channel modeling for intravehicle environment," *EURASIP J. Wireless Commun. Netw.–Special Issue Wireless Access Veh. Environ.*, vol. 2009, pp. 1–12, Jan. 2009.
[23] P. C. Richardson, W. Xiang, and W. Stark, "Modeling of ultra-wideband channels within vehicles," *IEEE J. Sel. Areas Commun.*, vol. 24, no. 4, pp. 906–912, Apr. 2006.
[24] T. Tsuboil, J. Yamada, N. Yamauchi, M. Nakagawa, and T. Maruyama, "Uwb radio propagation inside vehicle environments," in *Proc. Int. Conf. Intell. Transp. Syst.*, Jun. 2007, pp. 1–5.
[25] I. G. Zuazola, J. Elmirghani, and J. Batchelor, "High-speed ultra-wide band in-car wireless channel measurements," *IET Commun.*, vol. 3, no. 7, pp. 1115–1123, Jul. 2009.
[26] M. Schack, J. Jemai, R. Piesiewicz, R. Geise, I. Schmidt, and T. Kurner, "Measurements and analysis of an in-car uwb channel," in *Proc. IEEE VTC*, May 2008, pp. 459–463.
[27] W. Xiang, "A vehicular ultra-wideband channel model for future wireless intra-vehicle communications (ivc) systems," in *Proc. IEEE VTC*, Sep. 2007, pp. 2159–2163.
[28] C. U. Bas and S. C. Ergen, "Ultra-wideband channel model for intra-vehicular wireless sensor networks," in *Proc. IEEE WCNC*, Apr. 2012, pp. 42–47.
[29] C. U. Bas and S. C. Ergen, "Ultra-wideband channel model for intra-vehicular wireless sensor networks beneath the chassis: From statistical model to simulations," *IEEE Trans. Veh. Technol.*, vol. 62, no. 1, pp. 14–25, Jan. 2013.
[30] A. F. Molisch, "Ultra-wide-band propagation channels," *Proc. IEEE*, vol. 97, no. 2, pp. 353–371, Feb. 2009.
[31] M. Corrigan, A. Walton, W. Niu, J. Li, and T. Talty, "Automatic uwb clusters identification," in *Proc. IEEE RWS*, Jan. 2009, pp. 376–379.

Utku Demir received the B.S. degree in electrical and electronics engineering in 2012 from Koc University, Istanbul, Turkey, where he is currently working toward the M.S. degree in electrical engineering with the Wireless Networks Laboratory, Department Electrical Engineering, under the supervision of Prof. S. C. Ergen.

His research interests include Ultra-Wideband channel characterization in wireless communication systems and intra-vehicular wireless sensor networks.

Mr. Demir received a Koc University Full Merit Scholarship in 2007 and a scholarship from the National Scientific and Technology Research Council of Turkey (TUBITAK) in 2012 for his graduate studies.

C. Umit Bas (M'12) received the B.S. and M.S. degrees in electrical and electronics engineering from Koc University, Istanbul, Turkey, in 2010 and 2012, respectively. Since 2012, he is working toward the Ph.D. degree with the Department of Electrical Engineering, University of Southern California, Los Angeles, CA, USA.

While pursuing the M.S. degree, he was a Research Assistant with the Wireless Network Laboratory. He is currently working on development of measurement and testing equipment for distributed wireless communications and propagation channels with ultra-wide bandwidth as a part of WiDeS group.

Mr. Bas received the Koc University Merit Scholarship in 2005 and scholarships from Koc University and the TUBITAK National Scientific and Technology Council of Turkey in 2010 for his graduate studies.

Sinem Coleri Ergen (M'13) received the B.S. degree in electrical and electronics engineering from Bilkent University, Ankara, Turkey, in 2000 and the M.S. and Ph.D. degrees in electrical engineering and computer sciences from University of California, Berkeley, CA, USA, in 2002 and 2005, respectively. She was a Research Scientist with the Wireless Sensor Networks Berkeley Lab under the sponsorship of Pirelli and Telecom Italia from 2006 to 2009.

Since September 2009, she has been an Assistant Professor with the Department of Electrical and Electronics Engineering, Koc University, Istanbul, Turkey. Her research interests are in wireless communications and networking with applications in sensor networks and transportation systems.

Dr. Ergen received the Turk Telekom Collaborative Research Award in 2011 and 2012, the Marie Curie Reintegration Grant in 2010, the Regents Fellowship from the University of California, Berkeley, in 2000, and the Bilkent University Full Scholarship from Bilkent University in 1995.